Conceptual core design and application of mobile symmetrical inserted heat pipe cooled traveling wave reactor

Kunfeng Ma, Po Hu*

School of Nuclear Science and Engineering, Shanghai Jiao Tong University, Shanghai, China

*Corresponding author, E-mail address: pohu@sjtu.edu.cn

Abstract: Heat pipe reactors use heat pipe for passive cooling and are highly suitable for the energy supply of decentralized markets. Traditional mobile heat pipe reactors have smaller power level and cannot satisfy the higher power requirement of decentralized areas. Mobile heat pipe cooled traveling wave reactor (HPTWR), which uses neutron traveling wave to realize the long-term operation, is an excellent candidate for decentralized markets. In the present work, a radial traveling wave technology and a symmetrical inserted heat pipe technology are applied in the HPTWR core and a mobile symmetrical inserted heat pipe cooled traveling wave reactor (SI-HPTWR) core is developed. The radial traveling wave technology can improve the breeding capability of core and reduce the radial power peaking factor of core. Besides, the symmetrical inserted heat pipe technology can effectively reduce the maximum core temperature. The 60 MW_{th} SI-HPTWR is capable of supporting an around 60-year operation. Compared with other traditional reactors, SI-HPTWR has the higher safety, better mobility and economic benefits in the electricity market and heat utilization of decentralized areas.

Keywords: Heat pipe reactor; Traveling wave reactor; Neutronics analysis; Thermal analysis; Economic benefits

1. Introduction

As both the global energy demands and threats from climate change increase, many countries have been making great efforts on developing nuclear energy [1]. In recent years, due to the high capital cost of traditional large commercial nuclear power plants and the need of supply electricity to small grids of decentralized areas, there is a trend to develop small units of nuclear reactors [2]. Among various nuclear reactors, Small Modular Reactors (SMRs) with less than 300 MW_e are very suitable for the decentralized areas (such as space exploration, remote mines, military based and island communities) [3]. Different from traditional large commercial nuclear power plants, the components of SMRs can be fabricated in a factory setting and then transported as modules to the remote areas for installation. Therefore, the total cost of the SMRs is greatly reduced though factory fabrication, short construction time and standardization for commercial deployment, which is competitive in the energy markets of decentralized areas [4-5]. The Strategic Insights report [6-7] estimated the SMRs demand, which has a larger market in the future. For example, China and the United States are the most potential for SMRs development and the corresponding power demand of new SMRs additions in China and the United States are 5 GWe and between 1 and 5 GWe in 2035 respectively [7].

Numerous SMRs have been developed in the past 20 years, which mainly are composed of the water cooled reactors [8-9], gas cooled reactors [10], liquid-metal cooled reactors [11], molten salt cooled reactors [12-13], and heat pipe cooled reactors [14]. Due to its higher power density, simpler constructions, lower manufacturing cost, and higher safety, the heat pipe reactor is very suitable for the energy supply in the decentralized areas [14-16]. The heat pipe reactor was originally developed for the space exploration projects in 1960 [17]. Because of the small transportation capacity of the rocket and high power requirement in the space exploration, the mass of heat pipe reactor system in the space exploration is designed as small as possible and the corresponding power level is designed as high as possible [18]. Recently, various small modular heat pipe reactors have been proposed to the decentralized areas on the earth. Los Alamos National Laboratory (LANL) developed a MegaPower reactor, whose core is mainly composed of 6 monolith blocks, 2112 fuel pins, 1224 heat pipes (HPs), radius and axial reflectors [19]. The reactor is capable of suppling 5 MW_{th} for 12 years. The radius and high of core are only 77.85 cm and 200 cm respectively, which could be

easily deployed by truck. To improve the power level and lifetime of core, Choi [20] optimized the HP diameter and core structure, and then developed an 18 MW_{th} hybrid micro modular reactor (HMMR) which is mainly composed of 18 fuel assemblies, radius and axial reflectors. The equivalent radius and height of core are 102.5 cm and 280 cm respectively. The solid core with 12% enriched UN fuel can continuously supple for a full-power system lifetime of 56 years. Then, Westinghouse developed an eVinci heat pipe reactor with 15 MW_e to the energy supplement of off-grid market in 2018 [21]. A symmetrical-ended HP (cooled zone on either sides of a single heated zone) is applied to the core to improve the heat transport limits of a single-ended HP. The core with UO_2 fuel (19.75% ^{235}U enrichment) has the potential to operate up to 10 years. In order to further improve the power level of core, a 125 MW_{th} Heat Pipe Encapsulated Nuclear Heat Source (HP-ENHS) reactor is developed by inserting two symmetrical independent HPs in each coolant channel of core [22]. The radius and axial length of core are 97.2 cm and 400 cm respectively. However, both the volumes and masses of HP-ENHS and HMMR cores are very large, which cannot be deployed by truck or airplane.

To realize the higher energy supply of decentralized areas, the developed heat pipe reactors require two characteristics of the mobile and higher power level. Many heat pipe reactors can be transported by the truck or airplane. However, the power levels of those reactors are relatively lower (less than 50 MW_{th}), which cannot satisfy the power requirements of the large decentralized areas. For example, the power demand of remote mining application is around 20 MW_e, which is around 57 MW_{th} under 35% thermoelectric conversion efficiency [23-24]. Therefore, a higher heat transport HP and axial traveling wave technologies are applied in heat pipe reactor, and a 70 MW_{th} heat pipe cooled traveling wave reactor (HPTWR) core has been developed in previous studies [25-26]. The maximum HP and fuel temperatures in the HPTWR core are around 1800 K and 2394 K respectively [26]. To reduce the maximum core temperature, the symmetrical insert HP technology will be also applied in the HPTWR core and a symmetrical inserted heat pipe cooled traveling wave reactor (SI-HPTWR) core will be developed. To improve the breeding capability and reduce the radial power peaking factor (PPF) of core, the SI-HPTWR core will be segmented radially into two fuel regions and a radial traveling wave in the core will be introduced. The lifetime, breeding capability, fuel and HP temperatures of SI-HPTWR core will be analyzed. Section 2 describes the geometry model of SI-HPTWR core and computational tool. Results are shown in Section 3. Section 4 shows the applications and advantages of SI-HPTWR. Section 5 gives the conclusions.

2. Methodology

2.1 Core model

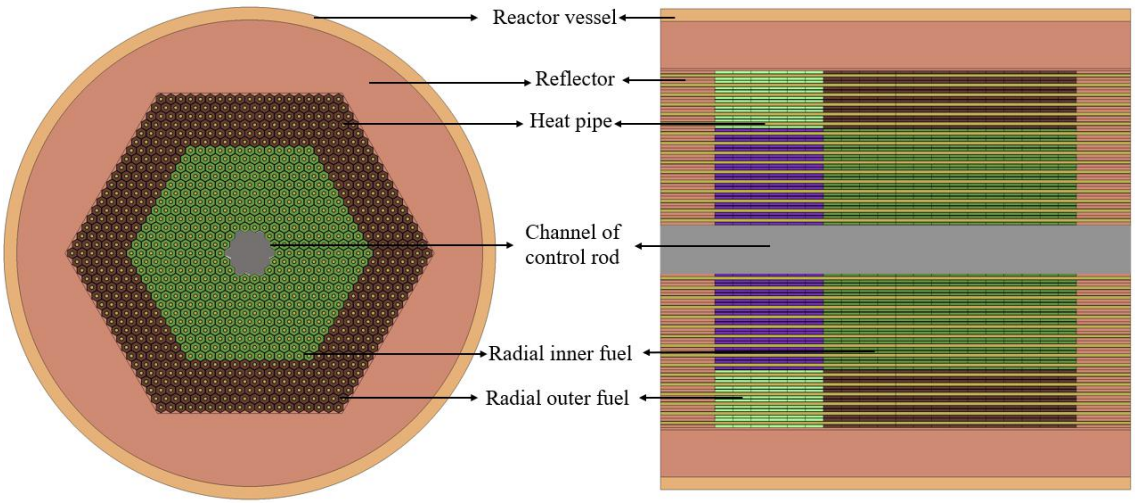

Fig.1 Radial and longitudinal layouts of SI-HPTWR core.

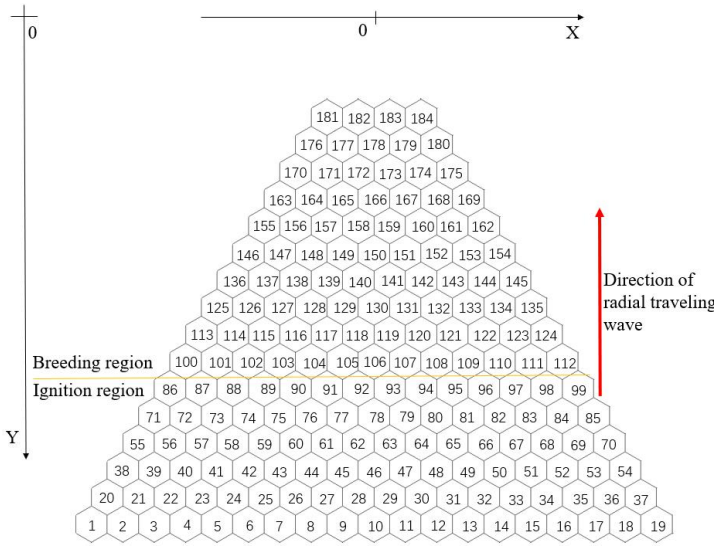

Fig.2 Radial FE loading of one-sixth core for SI-HPTWR.

The radial and longitudinal layouts of 60 MW_{th} SI-HPTWR core are showed in Fig.1 [26]. The core is the independent central HP fuel element (FE) design, which is radially composed of 1008 FEs. To realize the propagations of the axial and radial traveling waves, the core is segmented axially and radially into two fuel regions respectively. The axial lengths of axial ignition fuel region (IFR) and breeding fuel region (BFR) are 30 cm and 70 cm respectively. The FE amounts in radial inner and outer fuel regions are 450 and 558 respectively. In order to reduce the PPF of core, the radial ignition fuel and breeding fuel are loaded into the radial outer and inner fuel regions respectively. The radial FE loading of one-sixth core for the SI-HPTWR is showed in Fig.2. The lattice half-pitch of FE is 1.7128 cm and each FE is inserted into two independent HPs from the axial two sides (left and right). The Li HPs in the FE of SI-HPTWR core must be replaced during the entire cycle length because it has a relative shorter lifetime [20]. Based on the thermal power and HP amounts of core, the average HP temperature is around 1520 K. The corresponding vapor and liquid densities of Li in the gas channel and liquid annular of HP are around 3×10^{-5} g/cm^3 and 0.414 g/cm^3 respectively [27-28]. The specific parameters of FEs and HPs are listed in previous study [26]. 1008 FEs in the core contain 2016 HPs, which is surrounded by the radial and axial reflectors, and vessel. The radius and axial length of core are 90.3 cm and 130 cm respectively. The mass of SI-HPTWR core is around 29.04 tons (14.87 tons of fuel, 5.1 tons of cladding, 0.47 tons of HP, 7.65 tons of reflector and 0.95 tons of vessel), which can be easily transported by truck or airplane. Table 1 tabulates the design parameters of the SI-HPTWR core.

Fig.3 shows the nuclear system schematic of SI-HPTWR [22]. Each coolant channel of core is inserted two symmetrical independent HPs along two axial directions. The HP amounts in the SI-HPTWR core are double of those in the HPTWR core with single inserted HP [26]. Because the axial length of HP evaporation section in the core is shortened, the HPs irradiation damage in the SI-HPTWR core will be reduced relative to the HPTWR core in the case of same irradiation time. Therefore, the Li HPs in the SI-HPTWR core can realize a longer lifetime, which can reduce the replacement frequency of failure HP and improve the economy and safety of core.

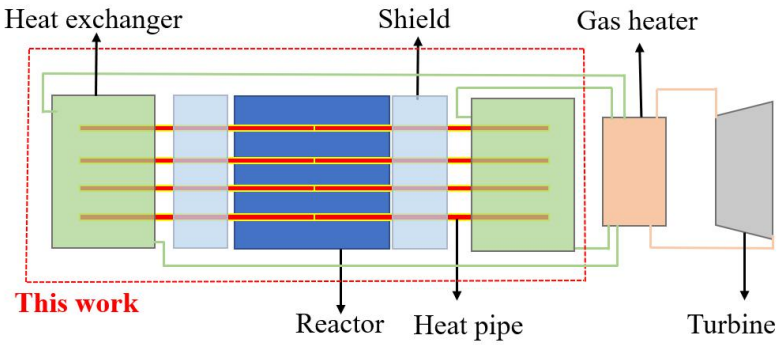

Fig.3 Nuclear system schematic of SI-HPTWR.

Table 1 Design parameters of SI-HPTWR core

Parameters	Value	Parameters	Value
Thermal power	60 MW_{th}	HPs amounts	2016
FEs amounts	1008	^{7}Li enrichment in Li HP	99.9%
Density of UN fuel	13.59 g/cm^3	Density of liquid Li in HP [27-28]	0.414 g/cm^3
^{15}N enrichment in UN fuel	95%	Density of vapor Li in HP [27-28]	3×10^{-5} g/cm^3
Thermal conductivity of UN at 1700 K [29]	24 W/(m·K)	Density of Al_2O_3 reflector	3.9 g/cm^3
Axial length of fuel	100 cm	Outer radius of reflector	90.3 cm
Mass of heavy nuclides	12.11 t	Axial length of reflector	15 cm
Density of Mo-14Re cladding	12 g/cm^3	Density of B_4C vessel	2.52 g/cm^3
Thermal conductivity of Mo-14Re at 1700 K [30]	70 W/(m·K)	^{10}B enrichment in B_4C vessel	90%

2.2 Computational tool

In the present work, Monte Carlo code RMC with ENDF/B-VII cross section library is used to perform the neutronic calculations, which is a code program developed by REAL team for neutron-photon-electron transport simulation [31-32]. The depletion simulations in the present work have 30000 neutrons per history with 400 batches and 50 discarded batches. The resulting standard deviation of k_{eff} for every depletion step is below 20 pcm. Both the powers of SI-HPTWR and HPTWR cores are set as 60 MW_{th}. Both the fuel and HP temperatures of SI-HPTWR and HPTWR cores in neutronics calculations are set as 1700 K to simplify the calculation based on the average UN temperature of 1700 K (see Section 4). In order to show the axial power profile, the fuel regions in two cores are segmented axially into 20 small depletion zones, and the axial length of small depletion zone is 5 cm.

The HP thermal calculations in the SI-HPTWR and HPTWR cores are executed by using the thermal resistance-capacitance network model (TreCan), which has been verified in previous study [26]. The HP evaporation section is segmented axially into 10 small zones, because the axial length of HP evaporation section is half of that of total fuel region. The axial FE power distribution is used as the heat source in the HP thermal calculations. The HP condensation section is cooled by the liquid metal Li. The temperature and velocity of liquid metal Li in the outside HP condensation section are set as 1470 K and 0.3 m/s respectively. When the Reynolds number (Re) is the range of from 10^4 to 10^5 for liquid Li cooling the axial cylinder, the Nusselt number (Nu) is accounted for through

$$Nu = 8 + 0.002 \times Re^{0.8}.\text{[33]} \quad (1)$$

Based on the Newton's cooling law, the heat transport of liquid Li in the HP condensation sections can be represented by

$$Q = \frac{Nu \times K_{cool}}{L_{cool}} \times S_{cool} \times (Tw - Tc). \quad (2)$$

Where the K_{cool}, L_{cool}, S_{cool}, T_w and T_c refer to the thermal conductivity of coolant (W/(m·K)), characteristic value of HP condensation sections (9.94 cm), surface area of HP condensation section (m^2), surface temperature of HP condensation section (K) and temperature of intermediate coolant (K) respectively. The axial lengths of HP adiabatic and condensation sections are set as 0.35 m and 1.0 m respectively. The HP evaporation section in the SI-HPTWR core is shortened to 0.5 m due to the application of symmetrical insert HP technology. The formulations of heat transport limits for Li HP can be found in previous study [26].

3.Results

3.1 U-Pu breeding

In previous study, we analyze the neutronic/thermal characteristics of the HPTWR core [26]. Different from

the HPTWR core, the symmetrical insert HP technology is applied in the SI-HPTWR and the core is segmented radially into two fuel regions. To show the effects of the symmetrical insert HP and radial traveling wave technologies to the core reactivity, both the initial k_{eff} of HPTWR and SI-HPTWR cores are set as around 1.0000 by adjusting the ^{235}U enrichments of every fuel region. Table 2 shows the ^{235}U enrichments of UN fuel for every fuel region in the HPTWR and SI-HPTWR cores. Two cores have a same materials, geometries and power levels. The radial outer IFR in the SI-HPTWR core has a larger neutron leakage relative to the HPTWR core because of its higher ^{235}U enrichment. Therefore, the average ^{235}U enrichment (11.5%) in the SI-HPTWR core is slightly higher than the average ^{235}U enrichment (11.1%) in the HPTWR core. For two cores, Fig.4 shows the k_{eff} changes against the operation time. Because of breeding of breeding fuel, the positive reactivity inserted by the new generated fissile isotopes is higher than the negative reactivity inserted by the consumption of nuclear fuel and accumulation of fission product during the early cycle length [34]. Therefore, the k_{eff} of SI-HPTWR core first increases. Then, the k_{eff} of core gradually decreases because of the decrease of ^{235}U and ^{238}U inventories in the nuclear fuel. The maximum k_{eff} of the SI-HPTWR core is around 1.0082 during the cycle length, which is higher than maximum k_{eff} (around 1.0066) of the HPTWR core because a radial breeding wave is applied in the SI-HPTWR core (see Fig.7) and the breeding capability of core has been improved (see Fig.5). The SI-HPTWR core can be operated for around 60 effective full power years, which is higher than the lifetime (around 54 years) of HPTWR core. The swing range of k_{eff} for the SI-HPTWR core (around 0.82%) is less than 1% during the entire cycle length.

Table 2 ^{235}U enrichments of UN fuel for every region in HPTWR and SI-HPTWR cores

^{235}U enrichments	HPTWR	SI-HPTWR	
		Radial inner fuel region	Radial outer fuel region
Axial IFR	13.83%	13.22%	15.12%
Axial BFR	9.93%	9.32%	11.22%

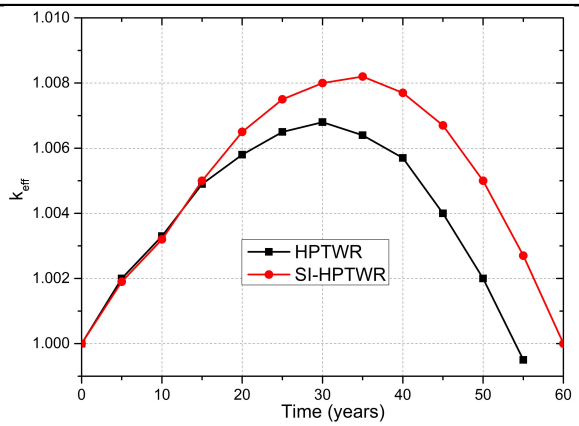

Fig.4 Changes of k_{eff} for SI-HPTWR and HPTWR cores during cycle length.

The inventories of nuclear fuel in the reactor core will be continuously decreased and new fissile Pu isotopes will be continuously accumulated for the U-Pu fuel cycle during the cycle length. Fig.5 (a) shows the ^{235}U inventories and consumptions in the SI-HPTWR and HPTWR cores during the cycle length. Due to it higher average ^{235}U enrichment, SI-HPTWR core has a higher initial ^{235}U inventory relative to the HPTWR core. The ^{235}U inventories in the SI-HPTWR and HPTWR cores are around 1.38 t and 1.33 t respectively at the beginning of cycle (BOC). Besides, the inventories of new bred fissile Pu isotopes gradually increase in two cores (see Fig.5 (b)), which can insert the positive reactivity. Therefore, the increase rates of ^{235}U consumptions gradually decrease in two cores during the cycle length. SI-HPTWR core has a slightly higher ^{235}U consumptions relative to the HPTWR core at same operation time because it has a higher ^{235}U inventory at the BOC. The ^{235}U inventories in the SI-HPTWR and HPTWR core are around 0.49 t and 0.51 t respectively at the end of cycle (EOC) and the corresponding ^{235}U consumptions are around 0.89 t and 0.82 t respectively at the EOC.

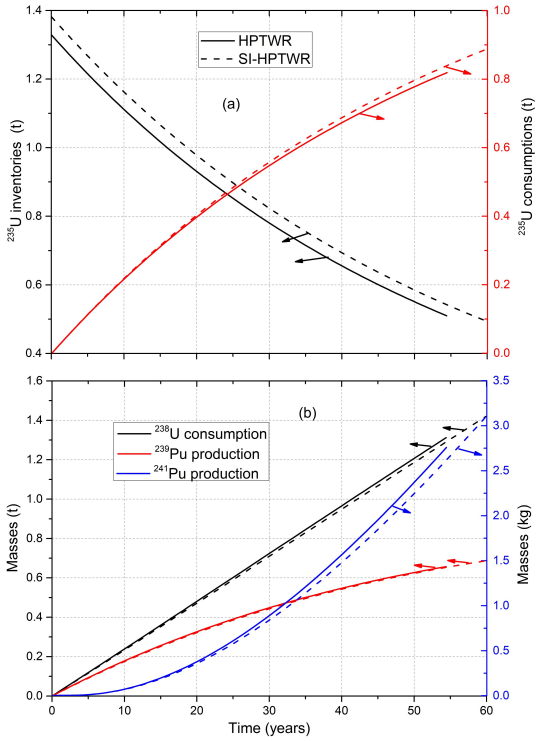

Fig.5 ^{235}U inventories and consumptions in SI-HPTWR and HPTWR cores during cycle length (a); ^{238}U consumptions, ^{239}Pu and ^{241}Pu productions in SI-HPTWR and HPTWR cores during cycle length (b).

Fig.5 (b) shows the ^{238}U consumptions, ^{239}Pu and ^{241}Pu productions in the SI-HPTWR and HPTWR cores during the cycle length. The ^{238}U consumptions in the SI-HPTWR and HPTWR cores are around 1.42 t and 1.31 t respectively at the EOC, and the corresponding ^{239}Pu productions are around 0.69 t and 0.66 t respectively. Besides, the corresponding ^{241}Pu productions are around 3.1 kg and 2.76 kg respectively at the EOC. The production rates of ^{239}Pu and ^{241}Pu in the two cores gradually increase and decrease respectively during the cycle length because the ^{238}U and ^{239}Pu inventories gradually decrease and increase respectively. The ^{238}U consumption, ^{239}Pu and ^{241}Pu productions in the SI-HPTWR core is lower than those in the HPTWR core at the same operation time because the SI-HPTWR core has a lower ^{238}U loading mass at the BOC. The ^{235}U consumption, ^{238}U consumption, ^{239}Pu and ^{241}Pu productions in the SI-HPTWR core during the cycle length is higher than those in the HPTWR core because SI-HPTWR core has a longer lifetime. To assess the breeding capability of U-Pu fuel cycle, the production fraction of fissile Pu isotopes can be evaluated by [25]

$$\mathrm{PF} = \frac{M_{\mathrm{Pu239}} + M_{\mathrm{Pu241}}}{M_{\mathrm{U238}}} \times 100\% \tag{3}$$

where M_{Pu239} and M_{Pu241} refer to the ^{239}Pu and ^{241}Pu productions in the core at the EOC respectively. M_{U238} refer to the ^{238}U inventory in the core at the BOC. The PF of SI-HPTWR core is around 6.46%, and slightly higher than the PF of HPTWR core (6.15%) during the entire cycle length because it has a higher U-Pu breeding capability (It can be also showed by the higher swing range of k_{eff} in Fig.4). The burnup of nuclear fuel in the SI-HPTWR core is around 108.33 GWd/MTU at the EOC, which is slightly higher than fuel burnup in the HPTWR core (98.42 GWd/MTU).

3.2 Power distribution

The SI-HPTWR core has two axial and radial fuel regions respectively. The IFR with higher ^{235}U enrichment will leak more fission neutrons to the BFR during the cycle length. The BFR with lower ^{235}U enrichment has a higher ^{238}U inventory, which can realize the higher breeding of ^{238}U during the cycle length. The burning of ignition fuel and breeding of breeding fuel in the SI-HPTWR core will lead to a change of axial and radial power profiles during the cycle length.

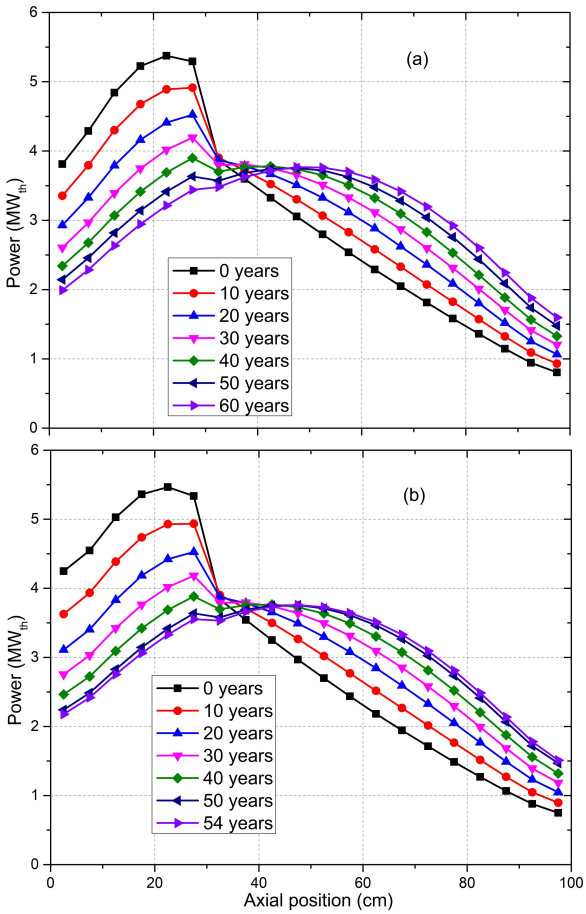

Fig.6 Axial power profile changes of SI-HPTWR core (a) and HPTWR core (b) during cycle length.

The axial power profile changes of SI-HPTWR and HPTWR cores are showed in Fig.6 (a) and (b) during the cycle length respectively. The SI-HPTWR and HPTWR cores have a same power level and fuel enrichment difference between axial IFR and BFR. Therefore, two cores have a similar axial power profile change during the cycle length. The axial peak power of SI-HPTWR core (around 5.38 MW_{th}) is slightly less than the peak power of HPTWR core (5.46 MW_{th}) at the BOC because the axial reflector along the axial IFR direction of the SI-HPTWR core is also inserted into HPs which leads to a larger neutron leakage during the cycle length. Due to the consumption of axial ignition fuel and breeding of axial breeding fuel, the axial peak powers of SI-HPTWR and HPTWR cores are reduced to around 3.76 MW_{th} and 3.77 MW_{th} at the EOC respectively. SI-HPTWR core has a smaller axial peak power at the EOC relative to HPTWR core because it has a longer lifetime. Both two cores have a same axial peak position at the BOC and EOC respectively, and the corresponding axial peak positions are around 22.5 cm and 47.5 cm respectively. The axial traveling wave speeds in the SI-HPTWR and HPTWR cores are around 0.4167 cm/years and 0.4630 cm/years during the entire cycle length respectively.

Different from the HPTWR core with the same radial fuel enrichment, the SI-HPTWR core has two radial fuel regions with different fuel enrichments. In order to explore the radial traveling wave characteristic, Fig.7 (a) and (b) show the radial normalized power profiles of one-sixth core in the SI-HPTWR at the BOC and EOC respectively. Because the radial IFR and BFR are loaded into the radial outer and inner positions of core respectively, the FE of radial IFR in the nearby radial BFR position has the maximum power distribution at the BOC. The maximum power FE is Nos. 92, and the radial distance between the centers of Nos. 92 FE and core is 43.11 cm. The corresponding radial PPF and the maximum FE power are around 1.118 and 66.55 kW_{th} respectively. The FEs in the nearby radial reflector position of core have a relatively higher power distribution at the BOC because more thermal neutrons are reflected by the radial reflector and ^{235}U has a larger thermal neutron fission cross section. Therefore, the FE power distributions in the radial outer IFRs first decrease and then increase as the core radius increases. More fission neutrons in the radius outer fuel region are diffused to the radius inner fuel region during the early cycle length and leaked to the radial reflector during the entire cycle length because it has a relatively higher power distribution. More ^{238}U

in the radius inner fuel region is bred into the Pu isotopes. More ^{235}U in the radius outer fuel region is consumed during the cycle length because it has a higher neutron leakage. Therefore, the FE power distributions in the radius inner fuel region and outer fuel regions gradually decrease and increase during the cycle length respectively. Besides, the neutrons leaked to the radial reflector in the SI-HPTWR core gradually decrease during the cycle length due to the decrease of power distribution of radial outer FEs. The SI-HPTWR has a relatively lower FE power distribution in the core's center at the BOC and EOC because the core's center has a safety rod channel. The maximum power FE is Nos. 173 at the EOC, which is in the radial inner fuel region. The SI-HPTWR core realizes the propagation of radial traveling wave during the entire cycle length. The radial distance between the centers of Nos. 173 FE and core is 16.57 cm. The corresponding speed of radial traveling wave in the SI-HPTWR core is around 0.4423 cm/year. Fig.8 shows the axial power profile changes of the radial IFR and BFR in the SI-HPTWR core at the BOC and EOC. The radial outer IFR has a higher power distribution at the BOC because it has a higher ^{235}U enrichment and FE amounts. The axial peak powers of radial IFR and BFR are around 2.80 MW_{th} and 2.58 MW_{th} at the BOC respectively. The nuclear fuel in the radial outer IFR and inner BFR of SI-HPTWR core are gradually consumed and bred during the cycle length respectively. Therefore, the power distribution of radial inner fuel region is higher than the power distribution of radial outer fuel region at the EOC. The axial peak powers of radial IFR and BFR are decreased to around 1.71 MW_{th} and 2.06 MW_{th} at the BOC respectively.

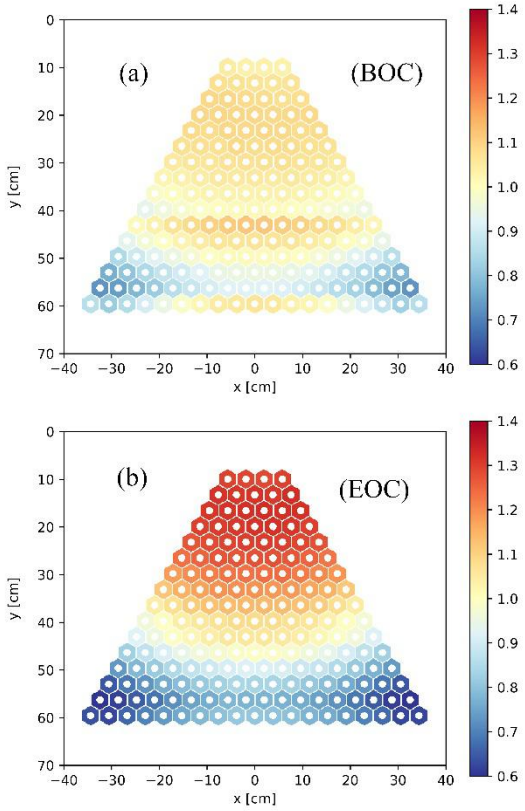

Fig.7 Radial normalized power profiles of one-sixth core in SI-HPTWR at EOC (a) and EOC (b).

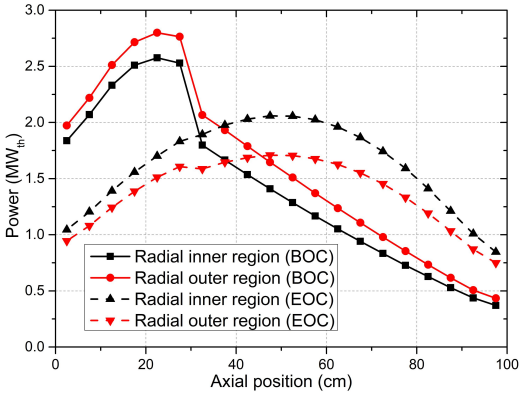

Fig.8 Axial power profile changes of radial IFR and BFR in SI-HPTWR core at BOC and EOC.

The normalized PPF and the corresponding FE power in the SI-HPTWR and HPTWR cores are showed in Fig.9 during the cycle length. The PPF of SI-HPTWR core is reduced to around 1.118 at the BOC relative to the HPTWR core (around 1.36) because the core is segmented radially into two fuel regions. The PPF of SI-HPTWR core is increased to around 1.327 at 50 years due to the breeding of radial inner fuel region. Many nuclear fuels in the radial inner breeding region have been consumed after 50 years. Thus, the normalized PPF is decreased to around 1.322 at 60 years. The corresponding FE power is increased from around 66.55 KW_{th} at the BOC to around 79.02 KW_{th} at around 50 years, and then decreased to around 78.67 KW_{th} at the EOC. The PPF of SI-HPTWR core is always lower than that of HPTWR core during the entire cycle length and thus the radial traveling wave technology can reduce the PPF of heat pipe reactor core. The axial power profile changes of the maximum power FE in the SI-HPTWR core are showed in Fig.10 during the cycle length. The axial power profiles of maximum power FE are similar to those of core (see Fig.6 (a)) during the cycle length. The axial peak power of maximum power FE is reduced from around 6.02 kW_{th} at the BOC to around 5.04 kW_{th} at the EOC, whose axial positions are 27.5cm and 52.5 cm respectively. The axial traveling wave speed of maximum power FE is consistent with that of power profiles of core.

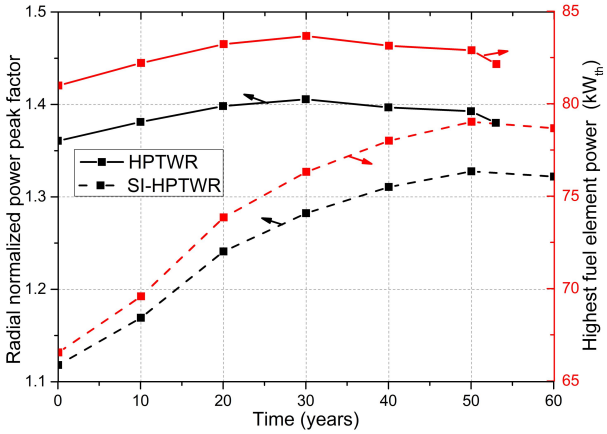

Fig.9 Radial normalized PPF and corresponding FE power in SI-HPTWR and HPTWR cores during cycle length.

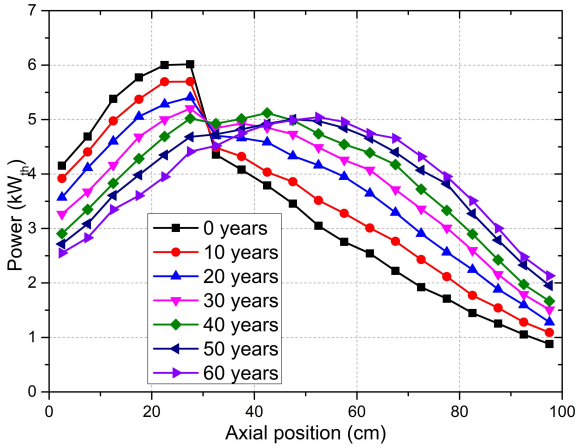

Fig.10 Axial power profile changes of maximum power FE in SI-HPTWR core during cycle length.

3.3 Temperature distribution

The symmetrical inserted HP technology in the heat pipe reactor can increase the HP amounts and the radial traveling wave technology can reduce the radial normalized PPF during the cycle length. To study the effect of the increase of HP amounts and decrease of radial normalized PPF to the core temperature, the thermal calculations of the Li HP and UN fuel are carried out by using the TreCan code and Fluent in the SI-HPTWR and HPTWR cores respectively [35].

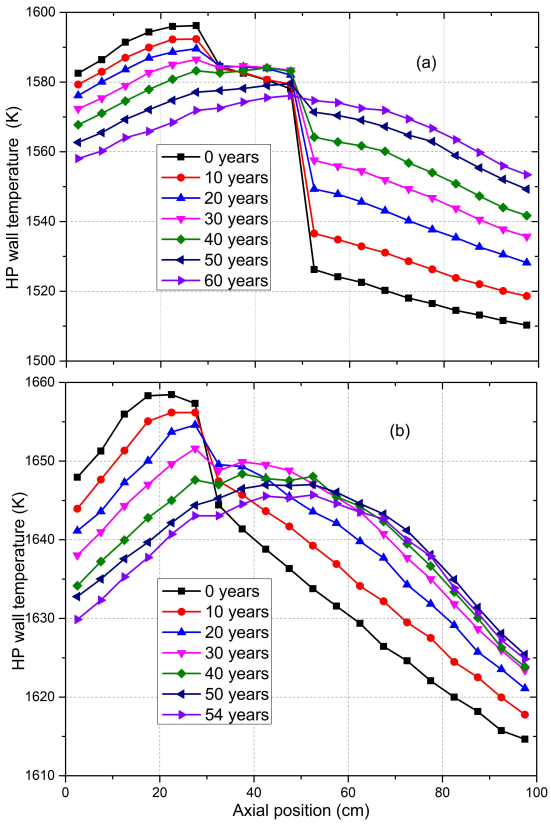

Fig.11 Axial HP wall temperature profile changes in maximum power FE of SI-HPTWR (a) and HPTWR (b) cores during cycle length.

Each FE in the SI-HPTWR core has two axial symmetrical inserted HPs relative to the HPTWR core with single inserted HP. To simplify the heat calculations, the junction of two axial symmetrical inserted HPs in one FE is set as adiabatic. Fig.11 (a) and (b) show the axial HP wall temperature profile changes in the maximum power FE of SI-HPTWR and HPTWR core during the cycle length respectively. For the SI-HPTWR core, the HP wall peak temperature and corresponding axial position are around 1596.17 K and 27.5 cm respectively at the BOC. The axial HP wall temperature profiles in the axial IFR and BFR directions gradually decrease and increase during the cycle length respectively because the corresponding axial FE power profiles gradually decrease and increase respectively (see Fig.10). The HP wall peak temperature is decreased to around 1579.53 K at the EOC, whose axial position is 47.5 cm. The peak temperature axial position in the maximum power FE is propagated from the axial IFR at the BOC to the axial BFR at the EOC. The HP wall peak temperature along the axial BFR direction in the maximum power FE of SI-HPTWR core is increased from around 1526.24 K at the BOC to around 1574.68 K at the EOC, whose axial position is always in 52.5 cm during the entire cycle length. The HP wall peak temperatures along the axial BFR direction are always less than those along the axial IFR direction during the entire cycle length. Because the junction of two axial symmetrical inserted HPs is located in the middle of core, the HP wall has a larger temperature difference in the axial junction of two HPs. The corresponding temperature difference is reduced from around 51.84 K at the BOC to around 1.43 K at the EOC because the axial power profile has a flattening during the cycle length. For the HPTWR core, the HP wall peak temperature is reduced from around 1658.45 K at the BOC to around 1645.70 K at the EOC. To explore the heat transport capability of the symmetrical inserted HP technology, Fig.12 shows the HP wall peak temperatures in the maximum power FE of the SI-HPTWR and HPTWR cores, and corresponding temperature difference during the cycle length. The HP wall peak temperature in the SI-HPTWR core is always less than the peak temperature in the HPTWR core during the cycle length and the corresponding peak temperature difference is increased from around 62.50 K at the BOC to around 67.50 K at around 50 years. The average powers of FE and small fuel zone in the SI-HPTWR core are around 59.52 kW_{th} and 2.976 kW_{th} respectively. The average HP wall temperature in the SI-HPTWR core is reduced to around 1544.4 K relative to the HPTWR core (around 1594.4 K) due to the application of the symmetrical inserted heat pipe technology. The maximum HP wall

temperature in the SI-HPTWR core gradually decreases during the cycle length, which can effectively enhance safety of reactor.

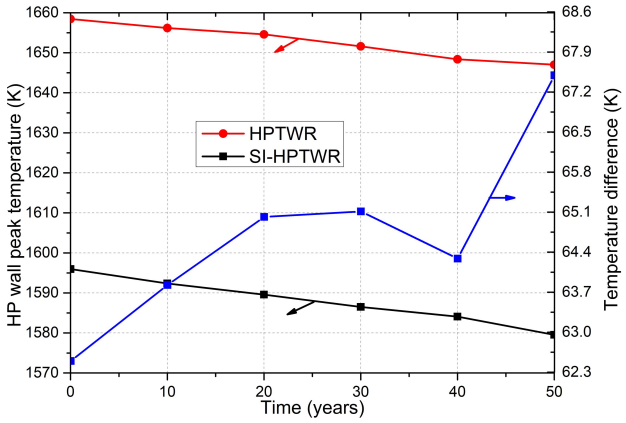

Fig.12 HP wall peak temperatures and corresponding temperature difference in maximum power FE of SI-HPTWR and HPTWR during cycle length.

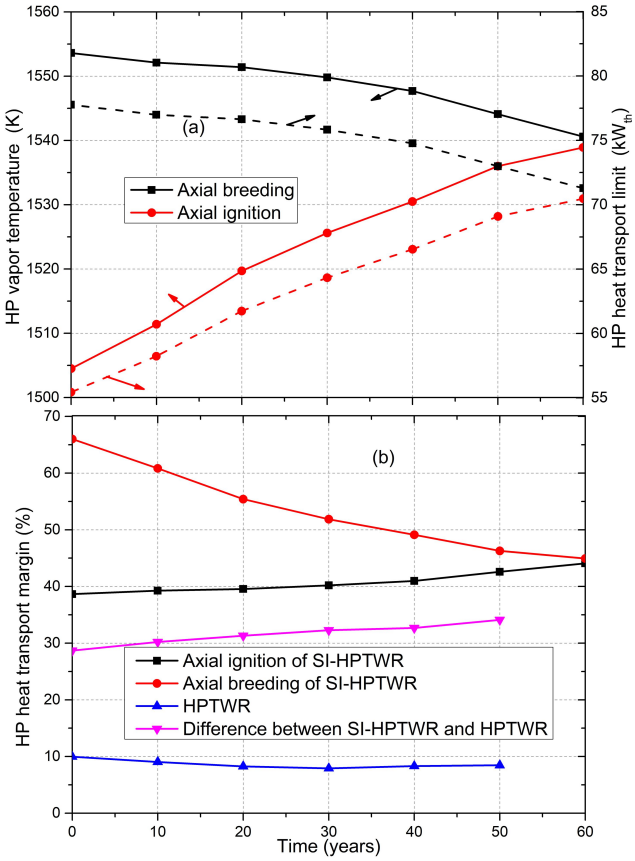

Fig.13 HP vapor temperatures and heat transport limits in maximum power FE of SI-HPTWR core during cycle length (a); HP heat transport margins and corresponding margin differences in the maximum power FE of SI-HPTWR and HPTWR cores during cycle length (b).

Based on the maximum power FE, the HP heat transport limits must be assessed to ensure the core heat transport during the cycle length. Fig.13 (a) shows the HPs vapor temperatures and corresponding heat transport limits in the maximum power FE of SI-HPTWR core during the cycle length. Fig.13 (b) shows the HP heat transport margins and corresponding margin differences in the maximum power FE of SI-HPTWR and HPTWR cores during the cycle length. The FE thermal power in the SI-HPTWR core will be transported by two axial symmetrical inserted HPs. Therefore, only half axial FE thermal power is transported by one HP. The HP vapor temperature is increased as the transported thermal power increases. The corresponding HP heat transport margin has a opposite varying trends. Thus, the HP vapor temperatures along the axial IFR and BFR directions are decreased and increased from around 1553.6 K and 1504.5 K at the BOC to around 1540.6 K and 1538.9 K at the EOC. The corresponding heat transport limits are

decreased and increased from around 77.76 kW_{th} and 55.44 kW_{th} at the BOC to around 71.28 kW_{th} and 70.47 kW_{th} at the EOC respectively. Besides, the corresponding heat transport margins are increased and decreased from around 38.66% and 66.01% at the BOC to around 44.08% and 44.93% at the EOC respectively. Due to the reduction of peak power, the minimum HP heat transport margins in the SI-HPTWR core gradually increase during the cycle length, which are always higher than those in the HPTWR core. The HP heat transport margin difference in the maximum power FE between SI-HPTWR and HPTWR cores is increased from around 28.69% at the BOC to around 34.12% at 50 years. Therefore, the symmetrical inserted HP technology and the radial traveling wave technology can effectively enhance the HP heat transport margin in the heat pipe cooled traveling wave reactor core.

Besides, the UN fuel temperatures in the SI-HPTWR and HPTWR core will be also assessed. Based on the core neutronics calculations and HP thermal calculations, the small fuel zone with the maximum and average powers in the SI-HPTWR and HPTWR cores will be calculated and the adiabatic boundaries are set at the outside surface of small fuel zone to simplify calculations. The heat transport through the gas gaps in FE is negligible because the gas gaps have a very small thickness [36]. The sensitivity analysis of mesh for the small fuel zone have been assessed in previous study [26]. The maximum fuel temperature in maximum power FE of SI-HPTWR core is first assessed. Fig.14 shows the radial (a) and axial (b) temperature profiles of maximum power small fuel zone in the SI-HPTWR core at the BOC. Because the central HP is surrounded by the radial fuel, the fuel temperature gradually decreases as the FE radius decreases. The axial fuel temperature profile remains basically unchanged because the axial length of small fuel zone is only 5 cm and the UN fuel has a higher thermal conductivity. The maximum fuel temperature is around 2024 K at the BOC [37]. Fig.15 shows the maximum fuel temperature in the HPTWR core, SI-HPTWR core, and corresponding temperature difference during the cycle length. The maximum fuel temperature in SI-HPTWR core is decreased to around 1925 K at the EOC and the decrease rate gradually decrease because the maximum fuel zone power gradually decreases during the cycle length. Based on the average small fuel zone power (2.79 kW_{th}) and corresponding HP wall temperature (1544.5 K), the average fuel temperature in the SI-HPTWR core is around 1700 K, which is less than the average temperature (around 1750 K) in the HPTWR core. The maximum fuel temperatures in the SI-HPTWR core are always less than the maximum fuel temperatures in the HPTWR core during the entire cycle length and the temperature difference is reduced from around 240 K at the BOC to around 78 K at 50 years. The symmetrical inserted HP technology and the radial traveling wave technology can effectively reduce the maximum fuel temperature during the cycle length.

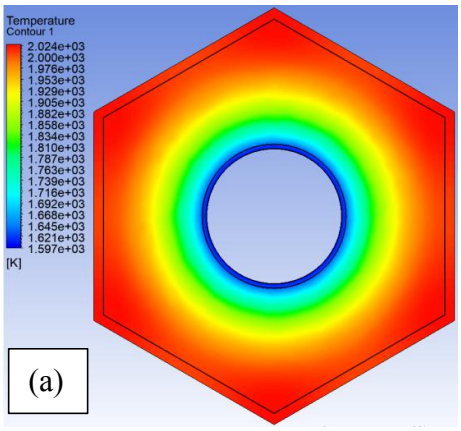

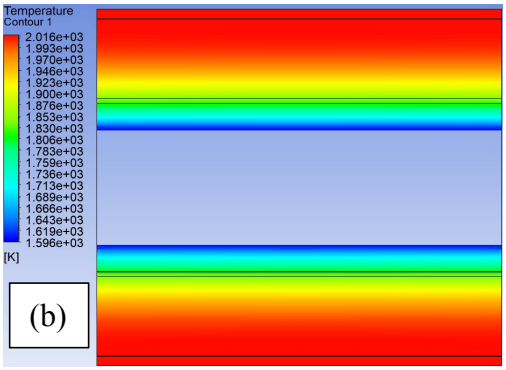

Fig.14 Radial (a) and axial (b) temperature profiles in maximum power small fuel zone of SI-HPTWR core at BOC.

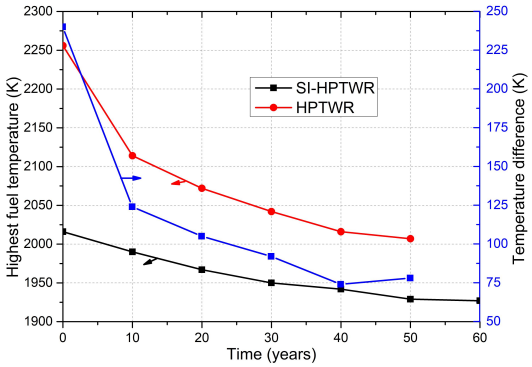

Fig.15 Maximum fuel temperatures and corresponding temperature differences in SI-HPTWR and HPTWR cores during cycle length.

4. Discussion

The symmetrical inserted HP technology and the radial traveling wave technology in the heat pipe reactor can effectively improve the safety of core. The mobile SI-HPTWR can realize 60 MW_{th} and 60 years continuous operation, which has a series of advantages relative to traditional reactors in the decentralized areas.

4.1 Safety of SI-HPTWR

The volumes of power system for the water, gas, liquid mental and molten salt cooled reactors are very large, and their construction cycle and cost are very long and high respectively. Many small manufactories cannot sustain the high cost. The use of HPs in the reactor shrinks the volume of power system, which is a key enabler for lowering the construction cost and investment risk. The SI-HPTWR does not require the main pipeline, circulating pump and auxiliary systems relative to traditional reactors with liquid or gas coolant, which results in a compact system. Therefore, the loss of coolant accidents and high pressure piping ruptures for the SI-HPTWR do not occur during the cycle length. Besides, the high mobility of SI-HPTWR can potentially simplify the requirements of siting factory and engineering tasks. Therefore, the SI-HPTWR can be easily installed underground by the transportation of truck, which further improves the security by the natural isolation of the containment area from external disruptors and releases. When some serious accidents occur, the SI-HPTWR power system can be fast transported to a safety region by the truck or airplane, which can reduce the maximum radiological harmfulness to the environment as well as human health.

4.2 Application of SI-HPTWR

The SI-HPTWR can not only support the household load but also realize the industrial demand on the earth, which have mainly two application fields in the decentralized areas, including electricity market and heat utilization.

(a) Electricity market

The levelized unit electricity cost of diesel in remote communities is in the range of \$0.466/kWh - \$0.487/kWh in Canada, which are composed of capital, operating, and decommissioning costs [38]. SMRs could provide an economically viable solution to deliver clean energy in the decentralized electrical markets. The levelized unit electricity cost of a 10 MW_e light water reactor has been decreased to around \$0.453/kWh (2015 US dollars) [1]. Relative to other SMRs with liquid or gas coolant, the devices of power system of

SI-HPTWR are smaller and the corresponding construction cycle will be shorted, which would further reduce the levelized unit electricity cost. The requirements of plant location for the SI-HPTWR are much less than those for other SMRs due to its high mobility. The SI-HPTWR can be transported at any time according to the need and the construction cost will be saved for the smaller electrical grids. Relative to the small grid with long distance transmission, the power disruptions during contingencies can be minimized or avoided by maintaining the continuous operation of SI-HPTWR. Besides, the application of SI-HPTWR in the decentralized areas can also eliminate the power transmission losses and provide increased resiliency. Due to the flexible siting attributes and firming power generation, the SI-HPTWR can also integrate with variable renewable energy to balance energy demands, and thus compensate the instability of wind, solar power and follow load. The power reserve requirements can be reduced by the application of SI-HPTWR, which can also provide the economic benefits in the decentralized areas.

(b) Heat utilization

The heat utilization in the decentralized areas mainly is composed of the process heat and district heating. The process heat with temperature ranging from 573 K to 1123 K are very common in a variety of industries (such as chemical and plastics manufacturing, food processing, petroleum refining, and hydrogen production and so on) [39]. By participating in wholesale power markets, 113 facility processes with 33.9 GWth/year thermal demand could be economically served by SMRs at 2021 US, which could avoid 4 million tons of CO_2 emissions per year [40]. The intermediate coolant temperature in the heat exchange of SI-HPTWR is 1470 K during the cycle length, which has a very high producing heat rate and is a suitable choice. Besides, the waste heat from nuclear generation (40-60 ℃) can be also applied to district heating systems, which increases the overall thermal efficiency of the plant and provides another revenue stream aside from electricity. District heating systems has a large market, which account for approximately 6% of global heat consumption [40]. For example, district heating systems supplies currently over 200 million persons in China and Russia [41]. In 2019, the market sizes of district heating in Europe and the Whole World were USD$137 billion and USD$173 billion respectively [42]. The network modifications are the major challenge to implementing a nuclear-fueled district heating system. In some regions, the costs of network modifications exceed 10 million Euros per kilometer, which may limit the application of conventional nuclear facilities situated far away from the denser population centers [43]. Therefore, when the mobile SI-HPTWR is applied, the distance piping network will be much shorted, which saves much cost of transmission network.

5. Conclusion

Based on the heat pipe cooling traveling wave reactor, the symmetrical inserted HP and radial traveling wave technologies are applied in the core to reduce the maximum core temperature and improve the breeding capability of core. The conclusions are as follows:

(1) The lifetime of 60 MW_{th} SI-HPTWR is around 60 years. The ^{239}Pu, ^{241}Pu productions and production fraction of fissile isotopes in the core are around 0.69 t, 3.1 kg and 6.46% during the entire cycle length respectively. The radial traveling wave technology can improve the breeding capability of core.

(2) The core can realize the propagations of axial and radial traveling waves during the entire cycle length, and the corresponding traveling wave speeds are around 0.4167 cm/years and 0.4423 cm/years respectively. The radial traveling wave technology can decrease the radial PPF of core.

(3) The maximum HP wall and fuel temperatures in the SI-HPTWR core are around 1579.53 K and 1925 K at the EOC respectively. The symmetrical inserted HP and radial traveling wave technologies can effectively reduce the maximum core temperature.

The SI-HPTWR has a good mobile and can provide economical service for the electricity market and heat utilization of decentralized areas.

Acknowledgement

The authors thank the National Natural Science Foundation of China for their support through Grant No. 11205098.

References

[1] D. Michaelson, J. Jiang, Review of integration of small modular reactors in renewable energy microgrids. Renew. Sustain. Energy Rev. **152**, 111638(2021). https://doi.org/10.1016/j.rser.2021.111638

[2] G. Locatelli, C. Bingham, M. Mancini, Small modular reactors: A comprehensive overview of their economics and strategic aspects. Prog. Nucl. Energy. **73**, 75-85(2014). https://doi.org/10.1016/j.pnucene.2014.01.010

[3] IAEA, Advances in Small Modular Reactor Technology Developments. Advanced Reactors Information System. (2014).

[4] N. Kaffezakis, T. Terlizzi, C. Smith, et al., High temperature ultra-small modular reactor: Pre-conceptual design. Ann. Nucl. Energy. **141**, 107311(2020). https://doi.org/10.1016/j.anucene.2020.107311

[5] X. Zhang, G. Huang, X. Zhou, et al., A multicriteria small modular reactor site selection model under long-term variations of climatic conditions -A case study for the province of Saskatchewan, Canada. J. Clean. Prod. **290**, 125651(2021). https://doi.org/10.1016/j.jclepro.2020.125651

[6] Strategic Insights, Small Modular Reactor Market (SMR) Outlook. (2015).

[7] G. Black, D. Shropshire, K. Araújo, Small modular reactor (SMR) adoption: Opportunities and challenges for emerging markets. Handbook of Small Modular Nuclear Reactors. 557-593(2021). https://doi.org/10.1016/B978-0-12-823916-2.00022-9

[8] M.H. Zahedi, G.R. Ansarifar, Design of a new Small Modular Nuclear Reactor using TVS-2M Fuel Assemblies and Fuel Depletion analysis during the fresh-core cycle length. Nucl. Eng. Des. **385**, 111540(2021). https://doi.org/10.1016/j.nucengdes.2021.111540

[9] A. Sadegh-Noedoost, F. Faghihi, A. Fakhraei, et al., Investigations of the fresh-core cycle-length and the average fuel depletion analysis of the NuScale core. Ann. Nucl. Energy. **136**, 106995(2020). https://doi.org/10.1016/j.anucene.2019.106995

[10] Z. Zhang, Y. Dong, F. Li, et al., The Shandong Shidao Bay 200 MWe High-Temperature Gas-Cooled Reactor Pebble-Bed Module (HTR-PM) Demonstration Power Plant: An Engineering and Technological Innovation. Engineering. **2**, 112-118(2016). https://doi.org/10.1016/J.ENG.2016.01.020

[11] S. Prasad, A. Abdulla, M.G. Morgan, et al., Nonproliferation improvements and challenges presented by small modular reactors. Prog. Nucl. Energy. **80**, 102-109(2015). https://doi.org/10.1016/j.pnucene.2014.11.023

[12] C. Zou, C. Yu, J. Wu, et al., Transition to thorium fuel cycle in a small modular molten salt reactor based on a batch reprocessing mode. Ann. Nucl. Energy. **138**, 107163(2020). https://doi.org/10.1016/j.anucene.2019.107163

[13] X. Zhao, Y. Zou, R. Yan, et al., Analysis of burnup performance and temperature coefficient for a small modular molten-salt reactor started with plutonium. Nucl. Sci. Tech. **34**, 17(2023). https://doi.org/10.1007/s41365-022-01155-2

[14] D. Wang, B. Yan, J. Chen, The opportunities and challenges of micro heat piped cooled reactor system with high efficiency energy conversion units. Ann. Nucl. Energy. **149**, 107808(2020). https://doi.org/10.1016/j.anucene.2020.107808

[15] J. Li, Q. Zhou, J. Mou, et al., Neutronic design study of an integrated space nuclear reactor with Stirling engine. Ann. Nucl. Energy. **142**, 107382(2020). https://doi.org/10.1016/j.anucene.2020.107382

[16] A. Wang, F. Shen, G. Hu, et al., A survey of heatpipe space nuclear reactor power supply. Nucl. Tech. **43**(06): 9-15(2020) https://doi.org/10.19328/j.cnki.1006-1630.2019.06.018 (in Chinese)

[17] G. Niederauer, E. Lantz, A split-core heat-pipe reactor for space power applications. NASA.TM X-52918:2(1970).

[18] M. Lee, G. Marc, P. Dave, "Kilowatt-Class Fission Power Systems for Science and Human Precursor Missions," Nuclear and Emerging Technologies for Space (NETS-2013). Albuquerque, New Mexico, February 25-28(2013).

[19] P. McClure, D. Poston, D.V. Rao, et al., Design of Megawatt Power Level Heat Pipe Reactors. LA-UR-15-28840(2015). https://doi.org/10.2172/1226133

[20] Y.J. Choi, S. Lee, S. Jang, et al., Conceptual design of reactor system for hybrid micro modular reactor (H-MMR) using potassium heat pipe. Nucl. Eng. Des. **370**, 110886(2020). https://doi.org/10.1016/j.nucengdes.2020.110886
[21] Westinghouse Electric Company, Westinghouse EVinci TM Micro Reactor. Accessed July (2018). https://doi.org/10.1115/ICONE28-67519
[22] E. Greenspan, Solid-Core Heat-Pipe Nuclear Battery Type Reactor. DE-FC07-05ID14706(2008). https://doi.org/10.2172/940911
[23] F. Caron, J. Abols, Production of electricity using small modular reactors (SMRs) for off-grid mining and other applications. Corpus ID:235802296(2020).
[24] K.S. Allen, S.K. Hartford, G.J. Merkel, Feasibility Study of a Micro Modular Reactor for Military Ground Applications. J. Def. Manag. **8**, 1(2018). https://doi.org/10.4172/2167-0374.1000172
[25] K. Ma, P. Hu, Preliminary conceptual design and neutroncis analysis of a heat pipe cooled traveling wave reactor. Ann. Nucl. Energy. 168, 108907(2022). https://doi.org/10.1016/j.anucene.2021.108907
[26] K. Ma, P. Hu, Preliminary neutronics and thermal analysis of a heat pipe cooled traveling wave reactor. Ann. Nucl. Energy. 190, 109876(2023). https://doi.org/10.1016/j.anucene.2023.109876
[27] D.W. Jeppson, J.L. Ballif, W.W. Yuan, et al., Lithium Literature Review: Lithium's Properties and Interactions, Hanford Engineering Development Laboratory. HEDL-TME, 78-115(1978). https://doi.org/10.2172/6885395
[28] IAEA-THPH, Thermophysical properties of materials for nuclear engineering: a tutorial and collection of data. International Atomic Energy Agency (2008).
[29] J.A. Webb, I. Charit, Analytical determination of thermal conductivity of W-UO_2 and W-UN CERMET nuclear fuels, J. Nucl. Mater. **427**, 87-94(2012). https://doi.org/10.1016/j.jnucmat.2012.04.020
[30] S.A. Fabritsiev, V.A. Gosudarenkova, V.A. Potapova, et al., Effects of neutron irradiation on physical and mechanical properties of Mo-Re alloys. J. Nucl. Mater. **191-194**, 426-429(1992). https://doi.org/10.1016/S0022-3115(09)80080-9
[31] K. Wang, Z. Li, D. She, et al., RMC- A Monte Carlo code for reactor core analysis. Ann. Nucl. Energy. **82**, 121-129(2015). https://doi.org/10.1016/j.anucene.2014.08.048
[32] Y. Ma, S. Liu, Z. Luo, et al., RMC/CTF multiphysics solutions to VERA core physics benchmark problem 9. Ann. Nucl. Energy. **133**, 837-852(2019). https://doi.org/10.1016/j.anucene.2019.07.033
[33] N. Uda, A. Miyazawa, S. Inoue, et al., Forced convection heat transfer and temperature fluctuations of lithium under transverse magnetic fields. J. Nucl. Sci. Techno. **38**, 11(2012). https://doi.org/10.1080/18811248.2001.9715120
[34] K. Ma, C. Yu, X. Cai, et al., Transmutation of ^{129}I in a single-fluid double-zone thorium molten salt reactor. Nucl. Sci. Tech. **31**:10(2020) https://doi.org/10.1007/s41365-019-0720-1
[35] Z. Wang, J. Gou, S. Xu, et al., Heat pipe failure accident analysis of a new type of megawatt heat pipe reactor. Nucl. Tech. 45(11):110-120(2022) https://doi.org/10.11889/j.0253-3219.2022.hjs.45.110604 (in Chinese)
[36] J.W. Sterbentz, J.E. Werner, A.J. Hummel, et al., Preliminary Assessment of Two Alternative Core Design Concepts for the Special Purpose Reactor. INL/EXT-17-43212(2018). https://doi.org/10.2172/1413987
[37] C. Chen, H. Mei, M. He, et al., Neutronics analysis of a 200 kWe space nuclear reactor with an integrated honeycomb core design. Nucl. Eng. Techno. **54**, 4743-4750(2022). https://doi.org/10.1016/j.net.2022.08.012
[38] M. Moore, The economics of very small modular reactors in the north. In: 4th international technical meeting on small reactors (ITMSR-4). Ottawa, ON (2016).
[39] M. Vanatta, D. Patel, T. Allen, et al., Technoeconomic analysis of small modular reactors decarbonizing industrial process heat. Joule. **7**, 4(2023). https://doi.org/10.1016/j.joule.2023.03.009
[40] International Energy Agency, How Can District Heating Help Decarbonise the Heat Sector by 2024?.

IEA Renewables. (2019).
[41] A.R. Mazhar, S. Liu, A.Shukla, A state of art review on the district heating systems. Renew. Sustain. Energy Rev. **96**, 420-439(2018). https://doi.org/10.1016/j.rser.2018.08.005
[42] Fortune Business Insights, District Heating Market Size, Share. Industry Growth [2020–2027]. No. FBI100097, 160(2020).
[43] F. Jasserand, L. J.G. D. Lavergne, Initial economic appraisal of nuclear district heating in France. EPJ Nuclear Sci. Technolo. **2**, 39(2016). https://doi.org/10.1051/epjn/2016028